Residual Heat in Ultra-Short Pulsed Laser Ablation of Metals

Franziska Bauer[*1], Andreas Michalowski[*1] and Stefan Nolte[*2]

[*1] Robert Bosch GmbH, Corporate Sector Research and Advance Engineering,
Postbox 30 02 40, 70442 Stuttgart, Germany
E-mail: franziska.bauer@de.bosch.com
[*2] Institute of Applied Physics, Abbe Center of Photonics, Friedrich-Schiller-Universität Jena,
Max-Wien-Platz 1, 07743 Jena, Germany

In ultra-short pulsed laser ablation of metals, a considerable amount of the incident laser energy remains in the workpiece as residual heat. When using high repetition rates, this can cause severe damage due to heat accumulation effects. In this paper, the amount and the spatial distribution of the residual heat deposited by a spatially Gaussian-shaped laser pulse are investigated by means of calorimetric measurements.

DOI: 10.2961/jlmn.2015.03.0016
Keywords: thermal effects, ultra-short pulses, laser ablation, micro processing, calorimetric measurements, heat accumulation

1. Introduction

The ablation of metals using ultra-short laser pulses enables processing with micrometer precision, a low surface roughness and a negligible heat-affected zone. This is primarily due to the fact that the energy of ultra-short laser pulses is deposited on a very short timescale. Thereby, strong non-equilibrium conditions are generated and the thermal diffusion length is in the same order of magnitude as the ablation depth [1-3]. This process is therefore often referred to as 'cold ablation'.

However, a considerable amount of the incident laser energy remains in the ambient bulk material as residual heat. Earlier work has shown that, when applying high repetition frequencies, this residual heat can lead to heat accumulation effects [4-7]. These can have a severe detrimental impact on the processing quality.

The objective of this research work is to quantify the total residual heat deposited by an ultra-short, spatially Gaussian-shaped pulse. As the thermal diffusion length for ultra-short pulsed laser processing is orders of magnitude smaller than the lateral dimensions of the laser spot, a surface heat source can be assumed. In this research, its spatial distribution $H_{\mathrm{res}}(x,y)$ is investigated. This is of particular interest for the simulation of sample heating during processing.

2. Experimental Design and Set-Up

In order to investigate the thermal energy deposited during the ablation of the stainless steel samples (EN steel number 1.4301), a calorimetric set-up is employed, as described in section 2.1.

The spatial distribution $H_{\mathrm{res}}(x,y)$ of the residual heat is determined by systematically varying the beam profile of the laser spot used for ablation. For this purpose, an ultra-short pulsed laser beam with a Gaussian intensity distribution is partly blocked using a copper blade and imaged on the workpiece for the laser ablation experiments (set-up illustrated in Fig. 4). The part of the laser spot contributing to ablation is then varied by moving the copper blade. The optical set-up used for the experiments is explained in more detail in section 2.2.

In the experiment, the laser spot is blocked beginning from a cut-off position x_0, as shown schematically in Fig. 1. For a given position x_0, the residual heat energy $E_{\mathrm{heat}}(x_0)$ remaining in the workpiece can be described by integrating the heat distribution $H_{\mathrm{res}}(x,y)$ as denoted in Eq. (1).

$$E_{\mathrm{heat}}(x_0) = \int_{-\infty}^{x_0} \mathrm{d}x' \int_{-\infty}^{+\infty} \mathrm{d}y'\, H_{\mathrm{res}}(x',y') = \int_{-\infty}^{x_0} \mathrm{d}x'\, \tilde{H}_{\mathrm{res}}(x') \tag{1}$$

Assuming radial symmetry for the spatial distribution $H_{\mathrm{res}}(x,y)$ of the residual heat, $\tilde{H}_{\mathrm{res}}(x)$ – the so-called line response function [8] – already contains the full information about $H_{\mathrm{res}}(x,y)$. As explained in [9], an Abel inversion can be performed to derive $H_{\mathrm{res}}(x,y)$ from the experimentally determined $E_{\mathrm{heat}}(x)$.

Concerning the laser beam source, a circularly polarized Yb:YAG disk laser (Trumpf GmbH + Co. KG, TruMicro5070) with a pulse duration of about $\tau = 6$ ps (FWHM, sech² fit) at $\lambda = 1030$ nm is used for the experiments. The laser spot is scanned across the workpiece using a galvanometer scanner (Intelliscan14de, SCANLAB AG).

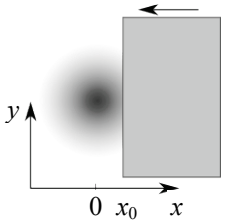

Fig. 1 Beginning from the cut-off position x_0, the laser spot is blocked.

2.1 Set-Up for Calorimetric Measurements

A standard calorimetric set-up is used to measure the residual heat, as depicted schematically in Fig. 2. The samples with lateral dimensions of 40 mm · 20 mm and a thickness of 1 mm are made of stainless steel (EN steel number 1.4301). A thin graphite foil brings the sample in thermal contact with a copper plate with the same lateral dimensions and a thickness of 0.5 mm. The high thermal conductivity of copper ensures a fast thermalization.

For the temperature measurement, a type T thermocouple (copper/constantan) is attached to the copper via a kapton tape. The components' masses and specific heats are listed in Table 1.

To obtain a slow temperature decay as required for this experimental method [12, 13], the sample is fixed on ceramic tips which ensures an adequate thermal isolation.

Table 1 Mass m and specific heat c_p at $T = 25°C$ of the components of the calorimetric set-up [10, 11].

material	mass m (g)	specific heat c_p (J/kgK)
stainless steel	6.45	472
copper	2.16	384
graphite foil	0.15	709

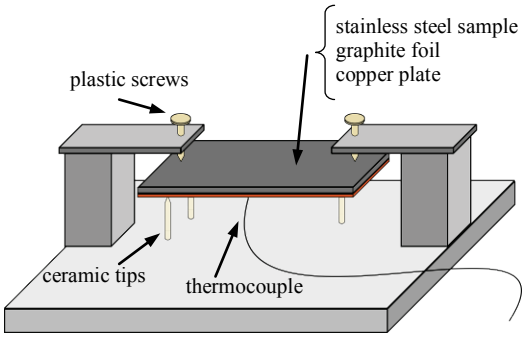

Fig. 2 Schematic drawing of the set-up used for the calorimetric measurements. Thermal energy is introduced by the ultra-short pulsed laser processing of the stainless steel sample.

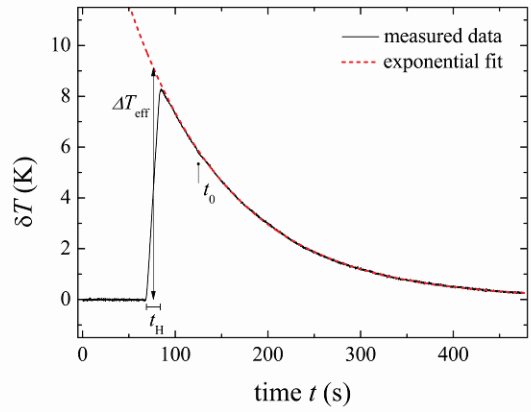

Fig. 3 Determination of the effective temperature rise ΔT_{eff} from the extrapolation of the exponential fit to the cool-down data.

For the calorimetric measurements, the sample is processed by a large number of pulses and thus heated during a time interval t_H. After thermalization (at t_0), the temperature decays exponentially. The relation given in Eq. (2) can be used to fit the logged temperature data.

$$T(t) = A_c + B_c \cdot e^{-\gamma_c (t - t_0)} \tag{2}$$

With the initial temperature A_c, the temperature change $\delta T(t)$ of the sample is then given by

$$\delta T(t) = T(t) - A_c . \tag{3}$$

As depicted in Fig. 3 and described in [12, 13], the effective temperature rise ΔT_{eff} of the workpiece can be approximated by extrapolating the exponential cool-down function to the middle of the heating interval:

$$\Delta T_{eff} = \delta T\left(\frac{t_H}{2}\right). \tag{4}$$

Knowing the respective heat capacities and the effective temperature rise ΔT_{eff}, the deposited thermal energy can be calculated [12, 13] according to

$$E_{heat} = \Delta T_{eff} \cdot \frac{0.5 \cdot \gamma_c \cdot t_H}{\sinh(0.5 \cdot \gamma_c \cdot t_H)} \sum_i c_p^{(i)} \cdot m^{(i)} . \tag{5}$$

The relative amount of the incident energy remaining in the workpiece as residual heat is given by

$$\%_{res} = \frac{E_{heat}}{E_{inc}} \cdot 100 , \tag{6}$$

where E_{inc} is the overall laser energy incident during the processing interval t_H.

2.2 Optical Set-Up

In order to investigate the spatial distribution $H_{res}(x,y)$ of the residual heat, $E_{heat}(x_0)$ is measured calorimetrically for different cut-off positions x_0, as described in section 2.1. The optical set-up used to partially block the laser spot is illustrated schematically in Fig. 4.

At a distance of about 1.7 m from the focusing lens of the scanning system (focal length $f = 163$ mm), a copper blade mounted on a translation stage is utilized to adjust the blocked fraction of the Gaussian beam (diameter $d = 2.6$ mm).

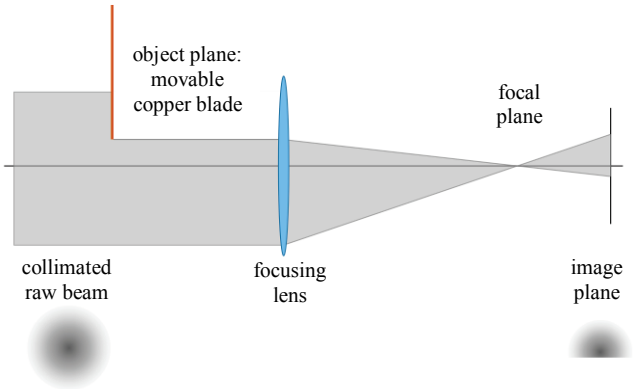

Fig. 4 Schematic illustration of the optical set-up: The collimated raw beam is partially blocked by a movable copper blade and imaged by the scanner focusing lens. The experiments are performed in the image plane.

The beam is imaged to the surface of the workpiece by the focusing lens. Here, the spot radius is found to be $w_{0,\,abl.} = (140 \pm 3)$ µm, measured according to the technique explained in [14].

In the image plane which is located about 17 mm behind the focal plane, an almost diffraction-free image of the partially blocked Gaussian beam can be observed. As depicted in Fig. 5, this has been verified with both beam profile measurements and the geometry of the ablation sites for different cut-off positions of the copper blade.

For the calorimetric measurements, a pulse repetition frequency of $f_{rep} = 20$ kHz and a pulse energy of $E_p = 460$ µJ are chosen. This results in an average fluence of $\varphi = 0.75$ J/cm², which is well above the ablation threshold fluence of stainless steel [15]. The average power hence is $P_{av} = 9.2$ W.

With a scanning speed of $v = 7$ m/s, lines with a length of 25 mm and a hatch line distance of 350 µm are processed on the stainless steel samples, providing for a separation of the single ablation sites. After 50 passes, the scanning program is finished after $t_H = 33.6$ s. Without blockage, the overall incident laser energy during the processing interval t_H amounts to $E_{inc} = 85$ J.

The calorimetric measurement is repeated for various cut-off positions x_0 of the copper blade, from free passage to complete blockage of the raw beam. Between the measurements, the blade is moved by $\Delta x_{obj.pl.} = 100$ µm which corresponds to a displacement in the image plane by $\Delta x_{im.pl.} = 10.8$ µm.

3. Results and Discussion

For each calorimetric measurement performed at a certain cut-off position x_0, the effective temperature rise ΔT_{eff} and γ_c result from the exponential fit using Eq. (2) and Eq. (4). The thermal energy $E_{heat}(x_0)$ and the relative amount $\%_{res}$ of the incident laser energy remaining in the workpiece as residual heat can then be calculated with the help of Eq. (5) and Eq. (6).

In Fig. 6, the experimental data of the residual heat E_{heat} is plotted against the cut-off position x_0 in the image plane from which on the spot is covered. As expected, the measured thermal energy $E_{heat}(x)$ increases when less of the raw beam is blocked by the copper blade.

To describe the experimental data mathematically, the error function ansatz given in Eq. (7) is found to be in good agreement with the experiment.

$$E_{heat}(x) = \frac{E_{heat,\,max}}{2} \cdot \left(1 + \mathrm{erf}\left(\frac{\sqrt{2}x}{w_{0,res.heat}}\right)\right) \qquad (7)$$

The resulting fit is depicted in Fig. 6 as a dashed line. It gives a value of $w_{0,\,res.heat} = (153.3 \pm 4.6)$ µm which – within the limits of this measurement technique – corresponds well with the spot radius of $w_{0,\,abl.} = (140 \pm 3)$ µm determined from the dimensions of the ablation sites in the image plane.

The first derivative of the fit to $E_{heat}(x)$ with respect to x – the line response function $\tilde{H}_{res}(x)$ – is Gaussian and therefore corresponds to a likewise Gaussian distribution of $H_{res}(x,y)$ [9]. Hence, we found that the spatial distribution of the residual heat $H_{res}(x,y)$ for a spatially Gaussian-shaped ultra-short laser pulse is also Gaussian with the same Gaussian root mean square width $w_{0,\,res.heat}$ as the ablating spot in the image plane $w_{0,\,abl.}$.

For ultra-short pulsed laser processing, there is a threshold fluence which has to be exceeded to ablate the material. Therefore, the absorbed energy, which has a spatially Gaussian distribution if the reflectivity does not depend on the applied fluence, can be subdivided into different parts – below and above the threshold for ablation [15].

In places where the fluence is below the threshold for ablation, the residual thermal energy is expected to be proportional to the applied fluence. In contrast to this, in places where the fluence exceeds the ablation threshold, a considerable part of the absorbed energy is expected to be carried away by the ablated particles. Therefore, a Gaussian distribution of the residual heat $H_{res}(x,y)$ is anything but obvious [e.g. 16].

Considering the overall amount of incident energy remaining in the workpiece as residual heat, the share is experimentally determined to be $\%_{res} = 34.0 \pm 2.3$. This value is in good agreement with the results reported in [17].

4. Conclusion

It was found that for the ablation of stainless steel, a considerable amount of the incident laser energy E_{inc} – as much as about one third – remains in the workpiece as residual heat.

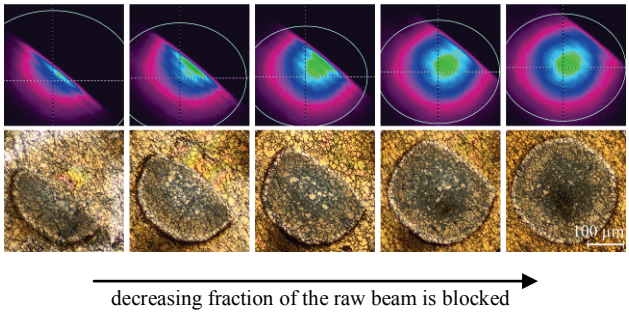

Fig. 5 Beam profile measurements (upper row) and ablation sites (lower row, $\varphi = 0.75$ J/cm²) on stainless steel in the image plane for different positions of the copper blade. In between the cases depicted above, the blade is moved by 0.4 mm.

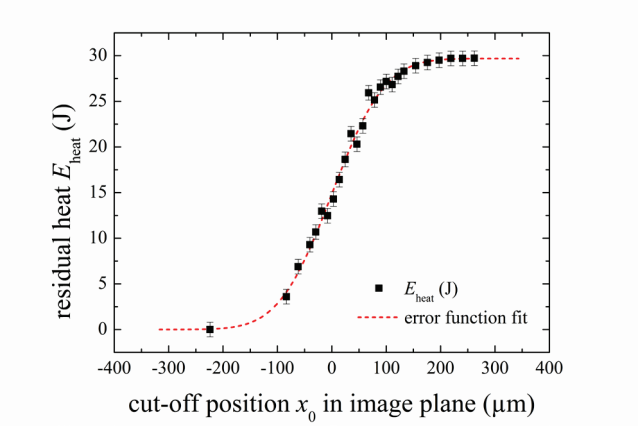

Fig. 6 Residual heat E_{heat} measured for different cut-off positions x_0. An error function ansatz is used to fit the data (dashed line).

For a spatially Gaussian-shaped ultra-short laser pulse, it is - against all expectations - a reasonable assumption that the spatial distribution $H_{res}(x,y)$ of the residual heat is also Gaussian with the same spatial extent. This information is crucial when computing the heat accumulation and the sample heating in ultra-short pulsed laser ablation of metals using high repetition frequencies [5].

References

[1] S. Nolte, C. Momma, H. Jacobs, A. Tünnermann, B. Chichkov, B. Wellegehausen and H. Welling: J. Opt. Soc. Am. B, 14, (1997) 2716.

[2] S. Preuss, A. Demchuck and M. Stuke: Appl. Phys. A Mater. Sci. Process., 61, (1995) 33.

[3] D. Bäuerle: "Laser Processing and Chemistry" (Springer, Berlin/Heidelberg, 2011) Chap. 13.

[4] R. Weber, T. Graf, P. Berger, V. Onuseit, M. Wiedenmann, C. Freitag and A. Feuer: Opt. Express, 22, (2014) 11312.

[5] F. Bauer, A. Michalowski, T. Kiedrowski and S. Nolte: Opt. Express, 23, (2015) 1035.

[6] S. Eaton, H. Zhang, P. Herman, F. Yoshino, L. Shah, J. Bovatsek and A. Arai: Opt. Express, 13, (2005) 4708.

[7] G. Raciukaitis, M. Brikas, P. Gecys and M. Gedvilas: Proc. SPIE 7005 – High-Power Laser Ablation VII, Taos, (2008) 70052L.

[8] J. Gaskill: "Linear Systems, Fourier Transforms, and Optics" (Wiley, New York, 1978), p. 339.

[9] R. O'Connell and R. Vogel: Appl. Optics, 26, (1987) 2528.

[10] D. Lide: "CRC Handbook of Chemistry and Physics" (CRC Press, Boca Raton, 2005), p. 4/135.

[11] SEW 310, "Physikalische Eigenschaften von Stählen" (Verlag Stahleisen GmbH, Düsseldorf, 1992).

[12] Deutsches Institut für Normung: "Charakterisierung von Laserstrahlen und Laseroptiken: Normen" (Beuth, Berlin, 2005), ISO 11551 .

[13] A. Michalowski: "Untersuchungen zur Mikrobearbeitung von Stahl mit ultrakurzen Laserpulsen" (Herbert Utz Verlag, München, 2014), Chap. 2.

[14] J. Liu: Opt. Lett., 7, (1982) 196.

[15] B. Neuenschwander, B. Jaeggi, M. Schmid, V. Rouffinage and P. Martin: Proc. SPIE 8243 – Laser Applications in Microelectronic and Optoelectronic Manufacturing, San Francisco, (2012) 824307.

[16] F. Dausinger, H. Hügel and V. Konov: Proc. SPIE 5147 – International Conference on Advanced Laser Technologies ALT-02, Adelboden, (2003) 106.

[17] A. Vorobyev and C. Guo: Opt. Express, 14, (2006) 13113.

(Received: May 22, 2015, Accepted: December 7, 2015)